Available online at www.sciencedirect.com
ScienceDirect
Journal of Theoretical Biology 242 (2006) 314–328
Journal of Theoretical Biology
www.elsevier.com/locate/yjtbi

A physical model for galvanotaxis of *Paramecium* cell

Naoko Ogawa[a,*], Hiromasa Oku[a], Koichi Hashimoto[b,c], Masatoshi Ishikawa[a]

[a]*Graduate School of Information Science and Technology, The University of Tokyo, Tokyo 113-8656, Japan*
[b]*Graduate School of Information Science, Tohoku University, Miyagi 980-8579, Japan*
[c]*PRESTO, Japan Science and Technology Agency, 4-1-8 Honcho, Kawaguchi-shi, Saitama 332–0012, Japan*

Received 7 September 2005; received in revised form 25 February 2006; accepted 27 February 2006
Available online 18 April 2006

Abstract

We propose a qualitative physical model of galvanotaxis of *Paramecium* cells using a bottom-up approach to link the microscopic ciliary motion and the macroscopic behavior of the cells. From the characteristic pattern of ciliary motion called the Ludloff phenomenon, the torque that orients the cell toward the cathode is derived mathematically. Dynamical equations of motion are derived and their stability is discussed. In numerical simulations using our model, cells exhibit realistic behavior, such as U-turns, like real cells.

Keywords: *Paramecium*; Galvanotaxis; Physical model; Ludloff phenomenon

1. Introduction

Galvanotaxis is an intrinsic locomotor response to an electrical stimulus, universally observed in diverse types of cells (Robinson, 1985), such as bacteria (Shi et al., 1996), amoebae and slime molds (Korohoda et al., 2000; Anderson, 1951), protozoa (Ludloff, 1895), and vertebrate cells including human tissue cells (Erickson and Nuccitelli, 1984; Orida and Feldman, 1982; Zhang et al., 2000; Fukushima et al., 1953; Gruler and Nuccitelli, 2000; Djamgoz et al., 2001). Recent studies have indicated that galvanotaxis may be involved in a number of biological phenomena (McCaig et al., 2005), such as embryo development (Erickson and Nuccitelli, 1984; Levin, 2003) and wound healing (Robinson, 1985; Chiang et al., 1992).

Ciliates, especially *Paramecium* cells, exhibit quite strong negative galvanotaxis (Machemer and de Peyer, 1977). That is to say, viewed macroscopically, the cell is forced to swim toward the cathode in a DC electric field. Since the first reports on galvanotaxis by Verworn (1889, 1896), pioneers in microbiology have eagerly investigated galvanotaxis of ciliates (Ludloff, 1895; Jennings, 1923; Kamada, 1929, 1931a,b; Kinosita, 1939). They found that galvanotactic movement is caused by a change in direction of the ciliary beating, in contrast to general cells, which move by elongation of actin filaments followed by rearrangement of the cytoskeleton (Mycielska and Djamgoz, 2004). This characteristic pattern of ciliary beating in *Paramecium* galvanotaxis is called the Ludloff phenomenon, explained qualitatively by Ludloff (1895). Since his original work, however, there has been almost no quantitative discussion of the physical relationship between the microscopic ciliary beating pattern and the macroscopic behavior of a cell. The purpose of this paper, therefore, is to propose a novel physical scheme for *Paramecium* galvanotaxis to provide a quantitative explanation for the Ludloff phenomenon, using a bottom–up approach based on systems theory.

Although several properties of *Paramecium* cells have been modeled, conventional models have mainly been physiological and biochemical ones that have focused on the membrane potential or signal transduction, ignoring the physical properties (Jahn, 1961; Cooper and Schliwa, 1985). Moreover, the few physical models that have been presented have tended to disregard galvanotaxis. For example, a physical model of the swimming behavior proposed by Naitoh and Sugino (1984) considered only the

*Corresponding author. Tel.: +81 3 5841 6937: fax: +81 3 5841 6952.
E-mail addresses: Naoko_Ogawa@ipc.i.u-tokyo.ac.jp (N. Ogawa), Hiromasa_Oku@ipc.i.u-tokyo.ac.jp (H. Oku), koichi@ic.is.tohoku.ac.jp (K. Hashimoto), Masatoshi_Ishikawa@ipc.i.u-tokyo.ac.jp (M. Ishikawa).
URL: http://www.k2.t.u-tokyo.ac.jp/.

0022-5193/$ - see front matter
doi:10.1016/j.jtbi.2006.02.021

behavior in the absence of an electrical stimulus. Though there are some physical *Paramecium* models based on gravitaxis or geotaxis (Fukui and Asai, 1980; Mogami et al., 2001; Hemmersbach et al., 2005), chemotaxis or chemokinesis (Houten and Houten, 1982; Sakane et al., 2001; Hirano et al., 2005), avoiding reaction (Sakane et al., 2001), calcium regulation (Laurent and Fleury, 1995), and thermotaxis (Oosawa and Nakaoka, 1977), they are not applicable to galvanotaxis, which is a side-effect of the electrophysiological properties of the membrane, a fundamentally different mechanism from other taxis or reactions. Fearing (1991) and Itoh (2000) independently performed pioneering experiments on controlling protozoa motion using galvanotaxis, but their approach was based on empirical rules. Some models on general taxis, that is, not limited to galvanotaxis in paramecia, are based on top–down qualitative mathematical assumptions rather than firm physical grounds (Schienbein and Gruler, 1993; Ohtake et al., 1997; Gruler and Nuccitelli, 2000; Ionides et al., 2003). One rare physical model of galvanotaxis is that constructed by Roberts (1970); however, its validity is uncertain because his assumptions were rough, and the accuracy of his model was not fully verified by comparing it with experimental data. This paper is the first attempt to construct a physical model of *Paramecium* galvanotaxis based on mechanics using a bottom–up approach, accompanied with experimental validation.

Our original motivation for this work stemmed from an engineering viewpoint; we have studied microrobotic applications of *Paramecium* cells, and have utilized galvanotaxis as a means of actuation of cells (Ogawa et al., 2005). The model that we propose in this paper was originally constructed in order to introduce the methodologies of robotics and systems theory based on physics for controlling cells, and it was found to be quite useful in controlling cells and trajectory planning. We believe that our model also has sufficient significance and novelty from a biological point of view.

2. Model of galvanotaxis

2.1. *Paramecium* and its galvanotaxis

2.1.1. Biological background

In this paper, we consider *Paramecium caudatum* because it has been extensively studied and its behavior is well known. *P. caudatum* is a unicellular protozoan with an ellipsoidal shape, inhabiting freshwater. It swims by waving cilia on its body; thousands of cilia beat the water backward to yield a forward reaction force (Naitoh and Sugino, 1984). The ciliary motion is controlled by shifts in the membrane potential and the accompanying changes in ion concentration in the cell.

When an external electrical stimulus is applied, it modifies the membrane potential and alters the ciliary movements, thus affecting the cell motion. Viewed macroscopically, the cell is made to swim toward the cathode. This phenomenon is called negative galvanotaxis. Note that galvanotaxis is simply a side-effect of the electrophysiological nature of the cell, unlike chemotaxis and phototaxis, which are behaviors conferring a survival advantage.

A *Paramecium* cell in an electric field shows a characteristic ciliary movement pattern. Assume an imaginary plane that is perpendicular to the electric field and located near the center of the cell, slightly closer to the cathodal end, dividing the cell into two parts, as illustrated in Fig. 1. The electric field causes cilia on the anodal end to beat more frequently (ciliary augmentation) (Kamada,

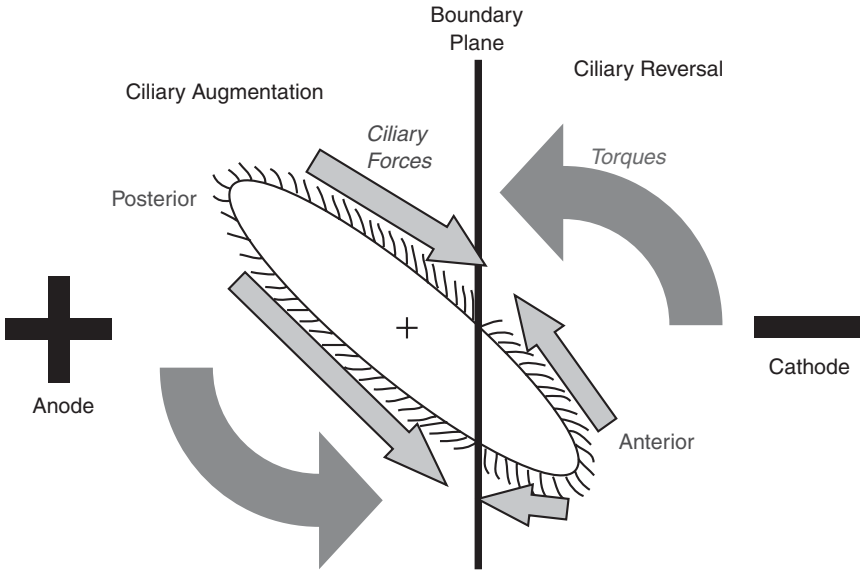

Fig. 1. Qualitative explanation for galvanotaxis. By applying an electric field, cilia on the anodal end begin to beat more frequently (ciliary augmentation) (Kamada, 1929), and cilia on the cathodal end beat more frequently but in the opposite direction (ciliary reversal) (Ludloff, 1895). The asymmetry in the ciliary beatings generates a rotational force and orients the cell toward the cathode.

1929), and the cilia on the cathodal end also beat more frequently but in the opposite direction (ciliary reversal) (Ludloff, 1895). This is called the Ludloff phenomenon, and it provides a simple and qualitative explanation for galvanotaxis: the asymmetry in direction of the ciliary beatings generates a rotational force and orients the cell toward the cathode.

Under weak electric field, the boundary between ciliary augmentation and ciliary reversal is located toward the cathode. This deviation is due to the interaction between the negative membrane potential ($\sim -30\,\mathrm{mV}$) and potential gradient distribution in the medium (Machemer and de Peyer, 1977; Görtz, 1988). Kamada (1931a,b) observed it and found that the boundary location changes slightly and inconsistently as the stimulus magnitude increases, which we do not consider in this paper for simplicity.

The Ludloff phenomenon was first described by Ludloff (1895). He concluded that this phenomenon was just an inorganic one caused by electromagnetic interaction between the electric current and the cilia, which is different from the current understanding based on electrophysiology.

Based on electrochemical and electrophysiological knowledge (Jahn, 1961; Cooper and Schliwa, 1985), the mechanism of the Ludloff phenomenon can be understood as follows:

1. When an electric field is applied, a voltage gradient appears from the anode to the cathode. According to electrochemistry, most of the gradient is concentrated near the regions called electric double layers formed near the electrodes, and only a slight gradient is produced in the bulk solution due to its electric resistance (Bergethon, 1998).
2. The gradient forms equipotential surfaces around the cell. Because the *Paramecium* cell surface itself is an equipotential and the body can be treated as a conductor (Eckert and Naitoh, 1970, 1972), the equipotential surfaces wrap around the cell, resulting in extremely strong fields at the anodal and cathodal ends.
3. At the cathodal end, the difference between intracellular and extracellular potentials decreases, which leads to depolarization. At the anodal end, the difference between intracellular and extracellular potentials increases, which leads to hyperpolarization (Cooper and Schliwa, 1985).
4. At the cathodal end, depolarization causes voltage-dependent Ca^{2+} channels (VDCCs) to be activated. Because the intracellular concentration of Ca^{2+} is extremely low, Ca^{2+} ions flow into the cell through the VDCCs, which causes further activation of the VDCCs (Naitoh et al., 1972). At the anodal end, hyperpolarization causes voltage-dependent K^+ channels (VDPCs) to be activated. Because the intracellular concentration of K^+ is higher, K^+ ions flow out of the cell through the VDPCs, which causes further activation of the VDPCs (Oertel et al., 1978).
5. At the cathodal end, depolarization and the increase in Ca^{2+} ion concentration cause ciliary reversal (Naitoh and Kaneko, 1972). At the anodal end, hyperpolarization causes ciliary augmentation (Machemer, 1974; Machemer and de Peyer, 1977). The precise reasons for these phenomena are still unknown.
6. Ciliary reversal and ciliary augmentation yield a backward force and a forward force, respectively. When the cell is tilted, therefore, the asymmetry of the two forces generates a torque.
7. The cell is directed toward the cathode by the torque. Consequently, the cell swims toward the cathode.

The mechanism described above shows that galvanotaxis is caused by electrochemical factors (1, 2), physiological factors (3, 5), and physical factors (6, 7). As discussed in Introduction, electrochemical and physiological factors have mainly been considered in previous studies. However, much remains unknown, and further theoretical studies cannot proceed without experimental data elucidating the structural and biochemical properties. On the other hand, though physical factors have not been considered sufficiently, they play an essential role in galvanotaxis and may be well described using simple physics. This paper concentrates on physical factors, while regarding electrochemical and physiological factors as "black boxes".

2.2. Assumptions

2.2.1. Simplification of cell motion

Strictly speaking, the motion of a *Paramecium* cell is composed of three elements as illustrated in Fig. 2: forward propulsion, a rotation around its longitudinal axis, and a rotation around its dorsoventral axis due to its asymmetrical shape. Consequently, the cell swims forward while spinning along a spiral (Naitoh and Sugino, 1984). The dominant element in galvanotaxis is the forward propulsion. For simplicity, we will not discuss the other two elements, which are not essential for galvanotaxis. Under this assumption, the cell simply moves straight ahead when there is no electric field.

By disregarding the rotational components, we can describe the cell motion in a two-dimensional plane including the cell axis and the electric field vector. Hereafter, we consider cell motion only in this plane. At the same time, because the motion of the cilia can be assumed to be symmetric with respect to this plane, the movements of the cilia in this plane can sufficiently represent the movements of all cilia. Thus, we consider the cell as a two-dimensional ellipsoid in this plane.

2.2.2. Coordinate systems

We define two coordinate systems on the plane, a global one (X, Y) and a local one (x, y), as shown in Fig. 3. The global coordinate system is allocentric, that is, fixed with respect to the external world, with the X-axis parallel to the electric field $\boldsymbol{E}$. The local coordinate system (introduced

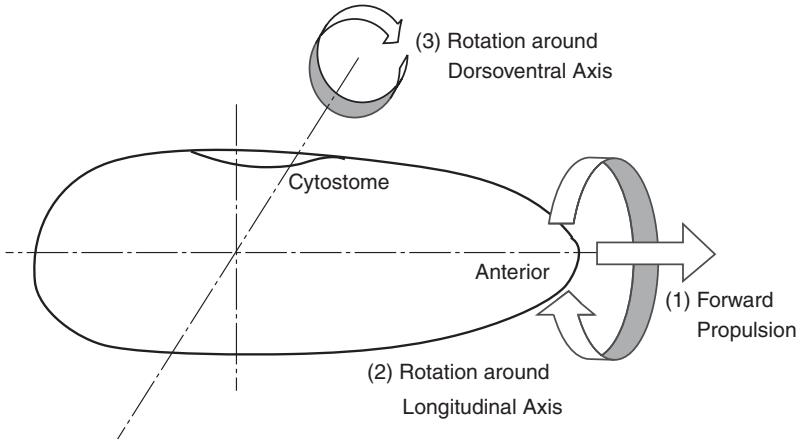

Fig. 2. Schematic representation of forces produced by movements of cilia. The motion of a *Paramecium* cell is composed of: (1) forward propulsion; (2) a rotation around its longitudinal axis, and (3) a rotation around its dorsoventral axis due to its asymmetrical shape. Reproduced from reference (Naitoh and Sugino, 1984) with modification.

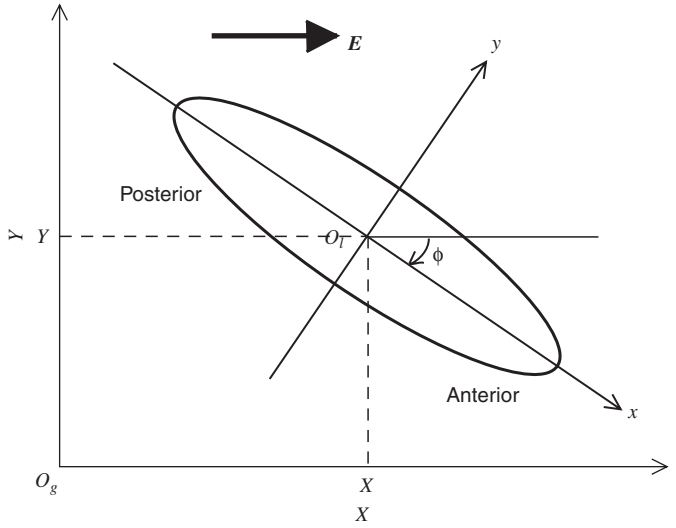

Fig. 3. Relation between the global coordinate system (X, Y) and the local coordinate system (x, y). The electric field E is applied along the X-axis. The cell is located at (X, Y) with tilt angle ϕ.

to simplify the description) is egocentric, that is, fixed with respect to the cell, with the x-axis parallel to the longitudinal axis of the cell. Let ϕ be the angle of the cell axis in the global coordinate system ($\phi<0$ in Fig. 3, for the sake of convenience in deriving the model).

We assume that the electric field is uniformly applied. Yamane et al. (2004) confirmed the validity of this assumption in a wide area by measuring the potential distribution in the solution.

Let the cell shape be an ellipsoid with a major axis of length $2L$ and a minor axis of length $2R$ ($L>R$). In the local coordinate system, the cell is represented as an ellipsoid $\mathscr{E}$:

$$\mathscr{E}: \frac{x^2}{L^2}+\frac{y^2}{R^2}=1. \quad (1)$$

2.2.3. Assumptions on ciliary motion

We assume that cilia are distributed uniformly around the edge of the ellipsoid with linear density n. For simplicity, we consider only two beating states, reverse and normal. The direction of the effective stroke in beating is oriented towards the anterior side in reverse beating, and towards the posterior side in normal beating. In the presence of an electric field, imagine a plane perpendicular to the field (hereinafter referred to as "a boundary plane"). This plane divides the cell into two regions; cilia beating is considered to be normal on the anodal side and reversed on the cathodal side. In common electrical stimuli, the boundary plane is formed towards the cathodal side (Kamada, 1931a). The shortest distance between the plane and the center of the cell is l, which is the offset of the boundary and should be smaller than R. We assumed l to be constant for simplicity in this paper.

The beating frequency of cilia is assumed to be uniform over the whole cell, with a value φ_0 in the absence of an electric field; this condition is hereinafter referred to as the "regular state". When an electric field E is applied, the frequency increases to $\varphi=(1+\beta E)\varphi_0$, where β is a positive parameter. This proportional relationship is approximately derived from the experimental results by Itoh (2000), where the swimming speed is approximately proportional to the electrical field, and from the fact that the beating frequency is approximately proportional to the membrane potential (Machemer, 1976). Let f_0 be the propulsion force yielded by one cilium in the regular state, the force being proportional to the frequency φ_0 (i.e. $f_0=\alpha\varphi_0$, where α is a positive coefficient). Let $f=\alpha\varphi=(1+\beta E)f_0$ be the force in the presence of the electric field.

2.3. Model of the torque

The phenomenon whereby a *Paramecium* cell swims toward the cathode is due to a torque caused by asymmetry

of ciliary motion. In this section, we estimate this torque. First, consider an ellipsoid $\mathscr{E}$ in the local coordinate system, as illustrated in Fig. 4. Note that the following model is defined only if $\boldsymbol{E} \neq \boldsymbol{0}$.

For convenience, let us introduce $\theta = -\phi$ as the angle of the electric field $\boldsymbol{E}$ in the local coordinate system. Then the boundary plane is expressed as a line $\mathscr{L}$:

$$\mathscr{L} : y = -\frac{1}{\tan\theta}x + \frac{l}{\sin\theta}. \tag{2}$$

The asymmetry of ciliary beating exists only at the substantially trapezoidal region formed by the intersection of the boundary plane and the ellipsoid (shown as the hatched region in Fig. 4. Draw two lines parallel to y-axis from the two intersection points of $\mathscr{E}$ and $\mathscr{L}$, and you will get two more intersecting points. The resulting four points make up the trapezoid). The forces yielded by cilia outside this region are symmetrical and do not contribute to rotation. Thus, we have only to consider the forces generated at this trapezoidal region.

The x-coordinates of two vertical lines that define the "upper" side and "lower" side of the trapezoid (that is, the sides parallel to the y-axis) are equal to those of two intersecting points of $\mathscr{E}$ and $\mathscr{L}$. These two coordinates, x_- and x_+, are obtained as two roots of the equation:

$$(R^2\sin^2\theta + L^2\cos^2\theta)x^2 - 2lL^2\cos\theta \cdot x + l^2L^2 - R^2L^2\sin^2\theta = 0, \tag{3}$$

which is derived by eliminating y from Eqs. (1) and (2) (obviously this equation always has two real roots). Let x_+ be the x-coordinate of the point with the larger y-coordinate and x_- be the x-coordinate of the point with the smaller y-coordinate.

Because it would be too complicated to consider the individual minute forces generated by each cilium, here we focus on the resultant forces for simplicity. We set the sites of action, $\mathrm{P}_1(x_a, y_a)$ and $\mathrm{P}_2(x_a, -y_a)$ $(y_a \geqslant 0)$, on the midpoints of the trapezoid edges, and assume the directions of the forces to be tangential to the ellipsoid. We define position vectors $\boldsymbol{r}_1 = \overrightarrow{\mathrm{OP}_1}$ and $\boldsymbol{r}_2 = \overrightarrow{\mathrm{OP}_2}$.

Then we obtain x_a (see Appendix B):

$$x_a = \frac{x_- + x_+}{2} = \frac{lL^2\cos\theta}{R^2\sin^2\theta + L^2\cos^2\theta}. \tag{4}$$

Also, y_a is obtained by substituting Eq. (4) into Eq. (1):

$$y_a = \frac{R}{L}\sqrt{L^2 - x_a^2}.$$

The two tangential lines at the sites of action $(x_a, \pm y_a)$ are given by

$$\frac{x_a}{L^2}x \pm \frac{y_a}{R^2}y = 1,$$

from which we get the inclinations of the two tangential lines,

$$m = \mp\frac{R^2 x_a}{L^2 y_a},$$

and normalized tangent vectors

$$\left(\frac{1}{\sqrt{1+m^2}}, \frac{m}{\sqrt{1+m^2}}\right) = \left(\frac{L^2 y_a}{\sqrt{R^4x_a^2 + L^4y_a^2}}, \mp\frac{R^2x_a}{\sqrt{R^4x_a^2 + L^4y_a^2}}\right).$$

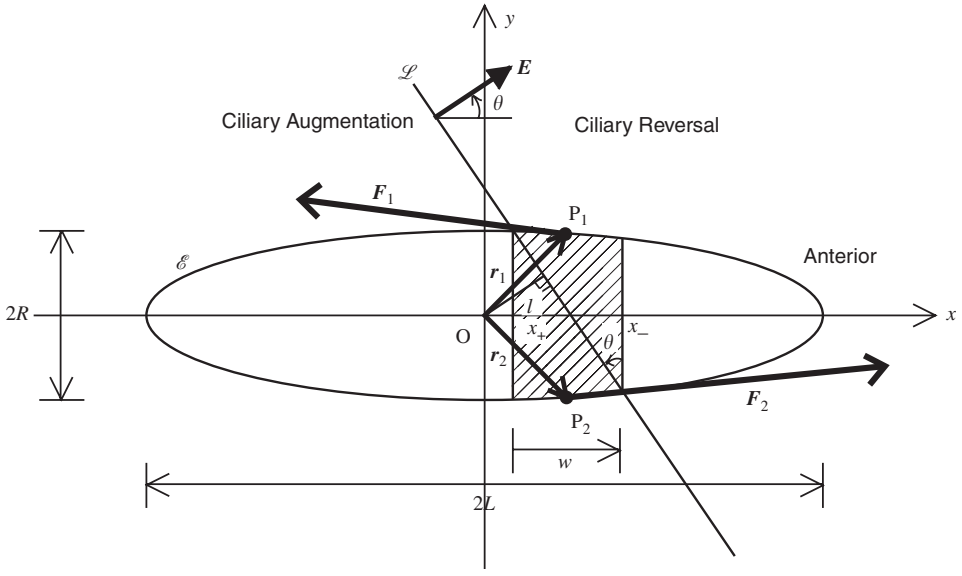

Fig. 4. Parameters in the local coordinate system. Only the cilia on the hatched trapezoidal region contribute to the rotation. $\mathscr{E}$: the cell represented as an ellipsoid; $2L$: the length of the cell; $2R$: the width of the cell; $\boldsymbol{E}$: the electric field; θ: the angle of the electric field; $\mathscr{L}$: the boundary plane perpendicular to the electric field; l: the offset of $\mathscr{L}$ from the local origin; x_+: the x-coordinate of the intersection of $\mathscr{E}$ and $\mathscr{L}$ (with positive y-coordinate); x_-: the x-coordinate of the intersection of $\mathscr{E}$ and $\mathscr{L}$ (with negative y-coordinate); w: the "height" of the trapezoid; P_1, P_2: the sites of action; $\boldsymbol{r}_1$, $\boldsymbol{r}_2$: position vectors for P_1 and P_2; $\boldsymbol{F}_1$, $\boldsymbol{F}_2$: the resultant forces yielded by the cilia.

Let $\boldsymbol{m}_1$ be the tangent vector at P_1 and $\boldsymbol{m}_2$ be that at P_2. Then unit force vectors, $\boldsymbol{e}_1$ at P_1 and $\boldsymbol{e}_2$ at P_2, are:

$$\boldsymbol{e}_1 = -\boldsymbol{m}_1 = \left(-\frac{L^2 y_a}{\sqrt{R^4 x_a^2 + L^4 y_a^2}}, \frac{R^2 x_a}{\sqrt{R^4 x_a^2 + L^4 y_a^2}} \right)$$

(for reverse beating),

$$\boldsymbol{e}_2 = \boldsymbol{m}_2 = \left(\frac{L^2 y_a}{\sqrt{R^4 x_a^2 + L^4 y_a^2}}, \frac{R^2 x_a}{\sqrt{R^4 x_a^2 + L^4 y_a^2}} \right)$$

(for normal beating),

considering the directions of the effective stroke in ciliary beatings.

Moreover, let us suppose that the magnitude of the resultant force is proportional to the "height" of the trapezoid, or w (see Appendix B):

$$w = x_- - x_+ = \frac{2RL \sin\theta \sqrt{R^2 \sin^2\theta + L^2 \cos^2\theta - l^2}}{R^2 \sin^2\theta + L^2 \cos^2\theta},$$

which is a signed value whose sign is the same as θ. Then the propelling forces $\boldsymbol{F}_1$ and $\boldsymbol{F}_2$ at the points P_1 and P_2, respectively, are written as:

$$\boldsymbol{F}_1 = fwn\boldsymbol{e}_1, \quad \boldsymbol{F}_2 = fwn\boldsymbol{e}_2.$$

By assuming that the center of mass of the cell is located at the center of the ellipsoid,[1] we find the torques at the points P_1 and P_2:

$$\boldsymbol{\tau}_1 = \boldsymbol{r}_1 \times \boldsymbol{F}_1, \quad \boldsymbol{\tau}_2 = \boldsymbol{r}_2 \times \boldsymbol{F}_2,$$

where it should be noted that these vectors are treated as three-dimensional in calculating cross products.

The torque rotating the cell body is given by:

$$\boldsymbol{\tau} = \boldsymbol{\tau}_1 + \boldsymbol{\tau}_2.$$

Since its x and y components are obviously zero, hereafter we call its z component, τ_z, the "torque".

Finally, by substituting $\phi = -\theta$, the torque is described in the global coordinate system as:

$$\tau_z(\phi) = -\frac{4LR^2 fns \sqrt{L^2 c^2 + R^2 s^2 - l^2}}{\sqrt{L^4 c^4 + 2L^2 R^2 c^2 s^2 + R^4 s^4 - L^2 l^2 c^2 + R^2 l^2 c^2}}, \tag{5}$$

where $s = \sin\phi$ and $c = \cos\phi$. This equation describes the torque generated in the cell oriented at the angle ϕ.

2.4. Forward propulsion force

As mentioned above, only the cilia on the trapezoid contribute to the rotation. Other cilia are responsible for translational propulsion. Considering that the reversed effective strokes on the cathodal side produce a backward force, we can derive the magnitude of the force F as:

$$F = \begin{cases} fn|[(L + x_+) - (L - x_-)]| = 2fn|x_a|, \\ \quad (|L \cos\theta| > 1), \\ fn|[(L + x_+) + (L - x_-)]| = fn(2L - |w|), \\ \quad (|L \cos\theta| < 1). \end{cases} \tag{6}$$

2.5. Equations of motion of paramecium cell

Using the torque estimated in Section 2.3, we now discuss the equations of motion of the *Paramecium* cell.

2.5.1. Equation of motion for translational motion

In the micrometer-scale world that paramecia inhabit, the inertial resistance of the fluid is small enough to be negligible, and the viscous resistance becomes dominant. This fact is also indicated by the small Reynolds number Re for a *Paramecium* cell, estimated as

$$Re = 2Lv/\nu = 0.10,$$

by using cell length $2L = 100\,\mu\text{m}$, velocity $v = 1\,\text{mm/s}$, and dynamic viscosity of water $\nu = 1.00 \times 10^{-6}\,\text{m}^2/\text{s}$. Hence we can apply Stokes' law, derived from the Navier–Stokes equation by ignoring inertial force.

Since a rigorous evaluation of the viscous resistance around an ellipsoid is quite complicated, here we approximate the viscosity by applying the formula for a sphere as a substitute. According to Stokes' law, the force exerted on a sphere with radius a, moving with velocity v in a viscous fluid is given by

$$F_s = 6\pi\mu a v, \tag{7}$$

where μ is the viscosity of the fluid. From this equation, the viscous force around the ellipsoidal cell can be obtained by replacing the radius a by the cell radius R. Thus the equation of motion for the translational motion of the cell can be approximated by:

$$M\ddot{\boldsymbol{X}} + D\dot{\boldsymbol{X}} = \boldsymbol{F}, \tag{8}$$

where $\boldsymbol{X} = (X, Y)^t$ is the cell position (a superscript t means the transposition), $\boldsymbol{F} = F\boldsymbol{e}$ is a forward propulsive force, $\boldsymbol{e} = (\cos\phi, \sin\phi)^t$ is a unit vector along the body axis, $D = F_s/|\dot{\boldsymbol{X}}| = 6\pi\mu R$ is the viscous friction coefficient, $M = \rho V$ is the cell mass, ρ is the cell density, and $V = 4\pi LR^2/3$ is the cell volume.

2.5.2. Equation of motion for rotational motion

We now derive an equation of motion for the rotational motion. As mentioned above, because evaluation of the viscosity around the ellipsoid is too complicated, we again substitute Stokes' law for a sphere. A viscous resistance torque against the rotation can be roughly approximated by assuming two mass points on the longitudinal axis at a quarter of the length $(L/2)$ from the origin, substituting $v = \dot{\phi} \cdot L/2$ and $a = L/2$ into the Stokes' law equation (7),

[1] It is reported that the center of mass is slightly deviated because of the fore-aft asymmetry under the condition that Reynolds number is so small (Mogami et al., 2001). However, we ignore the deviation for simplicity in this paper.

and multiplying both sides by $L/2$:

$$\tau_s = 2 \times F_s \frac{L}{2} = 12\pi\mu \frac{L}{2}\dot{\phi}\frac{L}{2}\frac{L}{2} = \frac{3}{2}\pi\mu L^3\dot{\phi}.$$

This derivation, however, may be too rough and the coefficient 3/2 might be unreliable, which may cause significant error in the model. Therefore, we introduce coefficient δ instead of the coefficient 3/2 to compensate for the error. Thus, the equation of motion for the rotational motion is given by

$$I\ddot{\phi} + D'\dot{\phi} = \tau_z(\phi), \tag{9}$$

where $I = \pi M(R^2 + L^2)/5$ is the moment of inertia for an ellipsoid, and $D' = \tau_s/\dot{\phi} = \delta\pi\mu L^3$ is the viscous friction coefficient.

2.5.3. Integration of equations of motion

Integration of the equations of motion for the translational motion (8) and the rotational motion (9) leads to the following equations with a notation common in systems theory:

$$\dot{\boldsymbol{q}} = A\boldsymbol{q} + \boldsymbol{B}(\boldsymbol{q}), \tag{10}$$

$$A = \begin{pmatrix} 0 & 0 & 1 & 0 & 0 & 0 \\ 0 & 0 & 0 & 1 & 0 & 0 \\ 0 & 0 & -D/M & 0 & 0 & 0 \\ 0 & 0 & 0 & -D/M & 0 & 0 \\ 0 & 0 & 0 & 0 & 0 & 1 \\ 0 & 0 & 0 & 0 & 0 & -D'/I \end{pmatrix},$$

$$\boldsymbol{B}(\boldsymbol{q}) = \left(0, 0, \frac{F}{M}\cos\phi, \frac{F}{M}\sin\phi, 0, \frac{\tau_z(\phi)}{I}\right)^{\mathrm{t}},$$

where $\boldsymbol{q} = (X, Y, \dot{X}, \dot{Y}, \phi, \dot{\phi})^{\mathrm{t}}$.

3. Numerical experiments

We performed some numerical experiments to verify the equations of motion using numerical analysis software (MATLAB, MathWorks Inc.).

3.1. Physical parameters

Table 1 shows several physical parameters used in the numerical experiments. We obtained the cell size by observing cells incubated in our laboratory; the size we observed was smaller than the average reported by Jennings (1923). The boundary plane offset l was estimated from several illustrations shown in previous studies (Jennings, 1923; Kamada, 1931a). The value of β, the increase in beating frequency with electric field, was estimated from the fact that the frequency increased to around 50 Hz under a stimulation of a few volts per centimeter from the frequency in the regular state of around 15–20 Hz (Naitoh and Sugino, 1984).

Table 1
Parameters of the proposed model

Parameters	Values	Comments
Major cell axis $2L$	100 μm	Our strain
Minor cell axis $2R$	25 μm	Our strain
Boundary plane offset l	10 μm	(Jennings, 1923; Kamada, 1931a)
Viscosity of water μ	1.00×10^{-3} kg/(ms)	At 20°C
Cell density ρ	1000 kg/m^3	Same as water
Increase in beating frequency β	2.00×10^{-3} V^{-1}	

The force yielded by cilia on the unit length, $f_0 n$, is still an unknown parameter. For rigorous evaluation, we might have to consider the physical model of a cilium (Sugino and Naitoh, 1982) and its interaction with the surrounding fluid. However, our model itself is based on approximation, and a strict evaluation of $f_0 n$ is not so critical. Hence we estimated the order of $f_0 n$ by using the swimming velocity measured in past experiments.

The terminal velocity of a cell in the regular state was obtained by substituting $\ddot{\boldsymbol{X}} = \boldsymbol{0}$ into Eq. (8) under conditions of $\phi = 0$:

$$\dot{\boldsymbol{X}} = \boldsymbol{F}/D = \frac{|x_a|_{\phi=0}\boldsymbol{e}}{3\pi\mu R} f_0 n. \tag{11}$$

Since x_a equals l at $\phi = 0$, we can estimate $f_0 n$ from:

$$f_0 n = \frac{3\pi\mu R}{l}|\dot{\boldsymbol{X}}|. \tag{12}$$

Measurement of the cell velocity by using a high-speed tracking system (Oku et al., 2005) described later in Section 3.8.1, gave a velocity of around 400 μm/s. Using this value, we estimated $f_0 n$ to be 4.71×10^{-6} N/m. In addition, we adjusted the parameter δ to be 7.5 based on experimental data of the cell trajectories obtained by our system (Ogawa et al., 2005).

3.2. Torque profile

Fig. 5 shows the torque $\tau_z(\phi)$ as a function of ϕ. Note that the torque affects the cell so as to decrease ϕ, that is, to make the cell turn toward the cathode.

These results indicate that the orientations $\phi = \pm\pi$ are kind of "singular point" where no torque is produced, even though the cell is oriented toward the anode. This means that such a cell will move towards the anode, which seems inconsistent with the observed behavior of negative galvanotaxis. In practice, however, swimming paramecia always sway slightly. The slight swaying of the cell generates a torque, causing the cell to incline further. This positive feedback rotates the cell and eventually directs it toward the cathode.

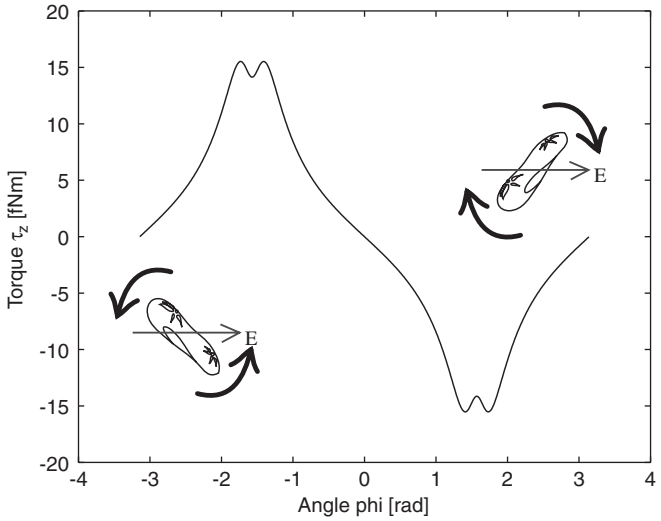

Fig. 5. Torque $\tau_z(\phi)$ generated by ciliary force. When $\phi>0$, a negative torque is generated to rotate the cell clockwise. When $\phi<0$, a positive torque is generated to rotate the cell counterclockwise. In both cases, the cell is eventually oriented toward the cathode.

3.3. Angular stability in the proposed model

Eqs. (8) and (9) indicate that the equations of motion of a *Paramecium* cell have a nonlinearity that might make the model unstable. However, when the angle ϕ is sufficiently small, that is, the direction of the cell is close to that of the electric field, it is possible to make the model approximately linear. In this section, we will linearize the model to observe the stability for small ϕ using methods commonly used in systems theory. Note that discussion on linearization is closed within this section and all numerical experiments described later were performed without linearization.

In Fig. 5, the z component of the torque, $\tau_z(\phi)$, exhibits a gradual monotonic decrease near $\phi = 0$, which implies that it can be regarded as linear with respect to ϕ in this area. Therefore, $\tau_z(\phi)$ can be approximated using the inclination of the tangential line at $\phi = 0$:

$$\tau_z(\phi) \simeq \left.\frac{\mathrm{d}\tau_z}{\mathrm{d}\phi}\right|_{\phi=0} \cdot \phi = -4\frac{R^2 Lfn\sqrt{L^2-l^2}}{\sqrt{L^4-L^2l^2+R^2l^2}}\phi.$$

Then Eq. (9) becomes:

$$\ddot{\phi} = -\frac{D'}{I}\dot{\phi} + \frac{Q}{I}\phi \quad \text{where } Q = -4\frac{R^2 Lfn\sqrt{L^2-l^2}}{\sqrt{L^4-L^2l^2+R^2l^2}}.$$

By defining a state variable $\tilde{\boldsymbol{q}} = (\phi, \dot{\phi})^{\mathrm{t}}$, the model of the cell rotation becomes linear around the origin $\tilde{\boldsymbol{q}} = \boldsymbol{0}$:

$$\dot{\tilde{\boldsymbol{q}}} = \tilde{A}\tilde{\boldsymbol{q}}, \quad \tilde{A} = \begin{pmatrix} 0 & 1 \\ Q/I & -D'/I \end{pmatrix}.$$

The eigenvalues of this matrix $\tilde{A}$ are the roots of the characteristic equation:

$$\det|\lambda I_{\mathrm{u}} - \tilde{A}| = 0,$$

where I_{u} is a unit matrix. Writing it as

$$\lambda^2 + \frac{D'}{I}\lambda - \frac{Q}{I} = 0,$$

and solving yields two roots $\lambda = \left(-D' \pm \sqrt{D'^2 + 4IQ}\right)/2I$, which we call λ_1 and λ_2.

Using Viète's Formulae providing the relation between roots and coefficients in polynomial equations (Viète, 1646), the sum and product of the two roots are derived from coefficients. Because D' and I are positive and Q is negative, their signs are determined as follows:

$$\lambda_1 + \lambda_2 = -\frac{D'}{I} < 0,$$

$$\lambda_1\lambda_2 = -\frac{Q}{I} > 0.$$

These results indicate that the real parts of both λ_1 and λ_2 are negative. Therefore, the cell is asymptotically stable for small ϕ and its direction converges to $\phi = 0$.

In addition, the global stability was verified qualitatively by calculating a potential energy U for rotation. We defined U as

$$\tau_z = -\frac{\partial U}{\partial \phi}$$

and computed it by numerical integration of Eq. (5) with respect to ϕ. Fig. 6 shows the profile of U, indicating that the cell is stable and tends to approach $\phi = 0$ for all ϕ.

3.4. Emergence of U-turn motion

When an electric field is applied in the direction opposite to the swimming direction of a cell, the cell makes a U-turn motion. We tested whether our proposed model can exhibit this phenomenon like real cells.

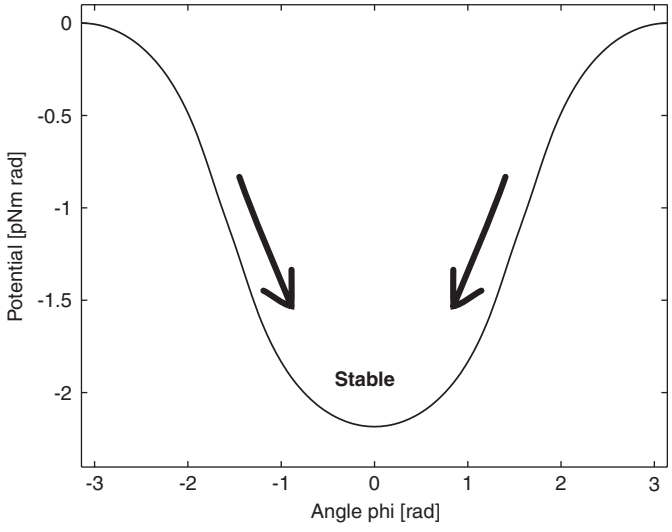

Fig. 6. Potential energy vs. torque, obtained by numerical integration of $\tau_z(\phi)$. The potential is minimized only at $\phi = 0$, indicating that the cell tends to approach $\phi = 0$ for all ϕ.

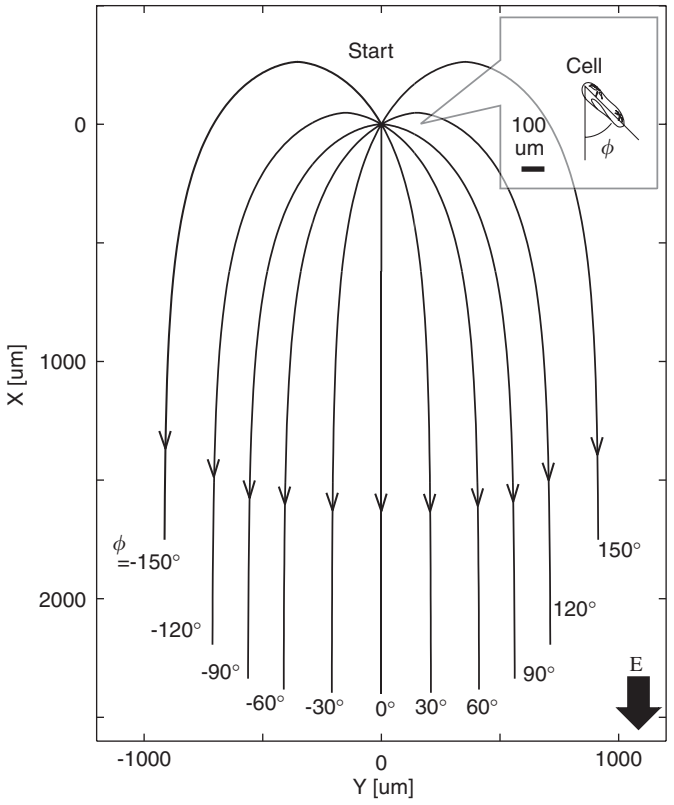

Fig. 7. Simulation of U-turn motions of cells. Swimming trajectories for cells with eleven different initial orientations are shown simultaneously. All cells were configured to have the same initial position, namely, on the origin $(0,0)$, but their initial angles ϕ differed by intervals of 30° $(-150°,-120°,\ldots,150°)$. A 5.0-V/cm electric field was applied along the X-axis. The trajectory of each cell was calculated by solving ordinary differential equations. All cells starting from the origin turned toward the cathode, like the real cells.

Swimming trajectories for cells with eleven different initial orientations were calculated. Fig. 7 demonstrates all trajectories simultaneously. All cells were configured to have the same initial position, namely, on the origin $(0,0)$, but their initial angles ϕ differed by intervals of 30° $(-150°,-120°,\ldots,150°)$. An electric field of 5.0 V/cm was applied along the X-axis. The trajectory of each cell was calculated by solving ordinary differential equations. As shown in Fig. 7, all cells starting from the origin turned toward the cathode, like real cells. It is interesting that realistic macroscopic behavior emerged from a microscopic description of the ciliary motion.

3.5. U-turn motion with spiral term and noise term

When the cell inclination ϕ is close to $\pm\pi$, Fig. 5 indicates that the torque is so small that the cell might fail to make an U-turn, or might need an extremely long time to turn. Actually, however, cells are certain to make an U-turn within short time. We think that it is due to the spiral path, as well as the perturbation of the cell angle caused by a noise. In this section, we consider incorporating a spiral motion, along with a noise term, into the simulation.

As mentioned in Section 2.2.1, the actual cell swims spinning along a spiral. The spiral path can be expressed as a sine curve (Naitoh and Sugino, 1984). To put it simply, it is written as:

$$\bar{X} = V_{\bar{X}} t,$$

$$\bar{Y} = V_{\bar{Y}} \cos \omega t,$$

where $\bar{X}$ correspond to the spiral axis whose direction is always oriented to the cell inclination ϕ, $\bar{Y}$ is an axis perpendicular to $\bar{Y}$, $V_{\bar{X}}$ and $V_{\bar{Y}}$ are amplitude coefficients, ω is the angular velocity, and t is time. Let $\bar{\phi}$ the cell inclination with respect to the $\bar{X}$ axis. Then,

$$\tan \bar{\phi} = \frac{\mathrm{d}\bar{Y}}{\mathrm{d}\bar{X}} = -\omega \frac{V_{\bar{Y}}}{V_{\bar{X}}} \sin \frac{\omega}{V_{\bar{X}}} t,$$

$$\bar{\phi} = \arctan\left(-\omega \frac{V_{\bar{Y}}}{V_{\bar{X}}} \sin \frac{\omega}{V_{\bar{X}}} t\right).$$

Because the spiral axis, or $\bar{X}$ axis, is always oriented to the swimming direction ϕ, the resulting cell angle is expressed as the sum of the path term ϕ and the spiral term $\bar{\phi}$:

$$\phi \leftarrow \phi + \bar{\phi}.$$

Finally, by considering a noise term N, the cell angle ϕ can be roughly enhanced as:

$$\phi \leftarrow \phi(1 + N).$$

We performed a numerical experiment. ω was set to be 2 according to the measurement (Ogawa et al., 2005). We also set N as a brown noise with the magnitude of 8.0×10^{-9}, and $V_{\bar{X}} = V_{\bar{Y}} = 1$. Other parameters were same as the U-turn experiment in Section 3.4. The initial angle was set to be 180°, which means that the cell was oriented to the anode.

Fig. 8 shows simulated trajectories for 10 trials. All cells made a full 180° U-turn motions and swam toward the cathode along the spiral path, although the torque was zero at the initial point.

3.6. Input-dependent behavior dynamics

Using our model, we can investigate how the response of a cell is influenced by the changes in the control inputs (the magnitude and direction of the electric field). This time, we focused on the time needed for the U-turn motion, named U-turn time. It is defined as the time from the initial position to the moment when it reached $\phi = 15°$. The default values for the magnitude of the electric field and the initial angle were set to 5 V/cm and 165°, respectively.

Fig. 9(a) shows the relation between the magnitude of electric field and the U-turn time, and (b) shows that between the angle of electric field and the U-turn time. The U-turn time decreased as the magnitude increased or the angle decreased, which agrees with the intuitive prediction.

Through our wet experiments, we know that the stronger field surely increases the percentage of cells moving toward

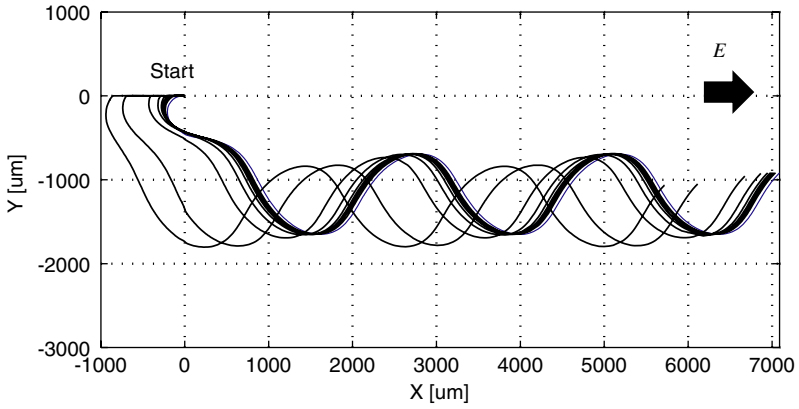

Fig. 8. Simulation of U-turn motions with a noise term and a spiral term for 10 different trials. All cells made a full 180° U-turn motions and swam toward the cathode along the spiral path, although the torque was zero at the initial point.

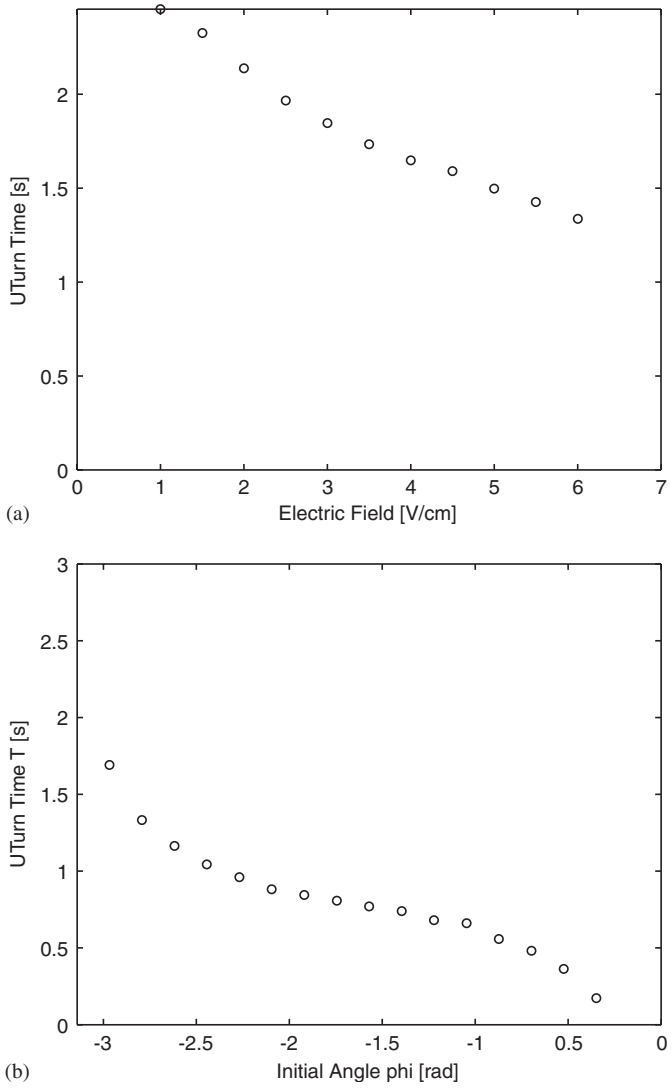

Fig. 9. (a) Relationship between the magnitude of the electric field E and the U-turn time. (b) Relationship between the electric field angle ϕ and the U-turn time. The U-turn time decreased as the magnitude increased or the angle decreased.

the cathode, but not all cells move perfectly in the electric field direction (cells die with more than 6 V/cm field in our experiments).[2] We attribute this incompleteness not to the instability of dynamics, but to the fluctuation of the membrane potential caused by complicated interaction between the field and cells or among cell themselves, which phenomenon is also widely observed under no electric field (Oosawa, 1975, 2001).

3.7. Shape-dependent behavior dynamics

In the numerical experiments described above, the parameter values were average values of multiple observed cells. However, there is significant intercellular variation, which may affect the macroscopic behavior. As an example, we varied the size parameters R and L to examine the effect on the behavior dynamics.

Fig. 10 shows the relationship between U-turn time and (a) L and (b) R. R was fixed to be 12.5 μm in (a) and L was fixed to be 50 μm in (b). It takes more time for more elongated cells to make a U-turn; this is thought to be because elongated shapes experience more resistance in rotation than spherical ones do.

Rotation and translation are quite common motions for paramecia, though their origin is not galvanotactic. The ellipsoidal shape of cells might be the result of evolution, with the trade-off that elongated bodies are favorable for translation but adverse for rotation.

It is implied that the shape deviation cannot be neglected for rigorous evaluation, though it gives almost no fundamental difference in the structure of the model and emerging behaviors. Note that our Stokes-like assumption in motion of equations has to be reconsidered from the

[2]As for other species, for example, 100% of Dictyostelium cells move directly toward the cathode under relatively strong field (~15–20 V/cm) (Zhao et al., 2002), though its mechanism is different from *Paramecium* galvanotaxis.

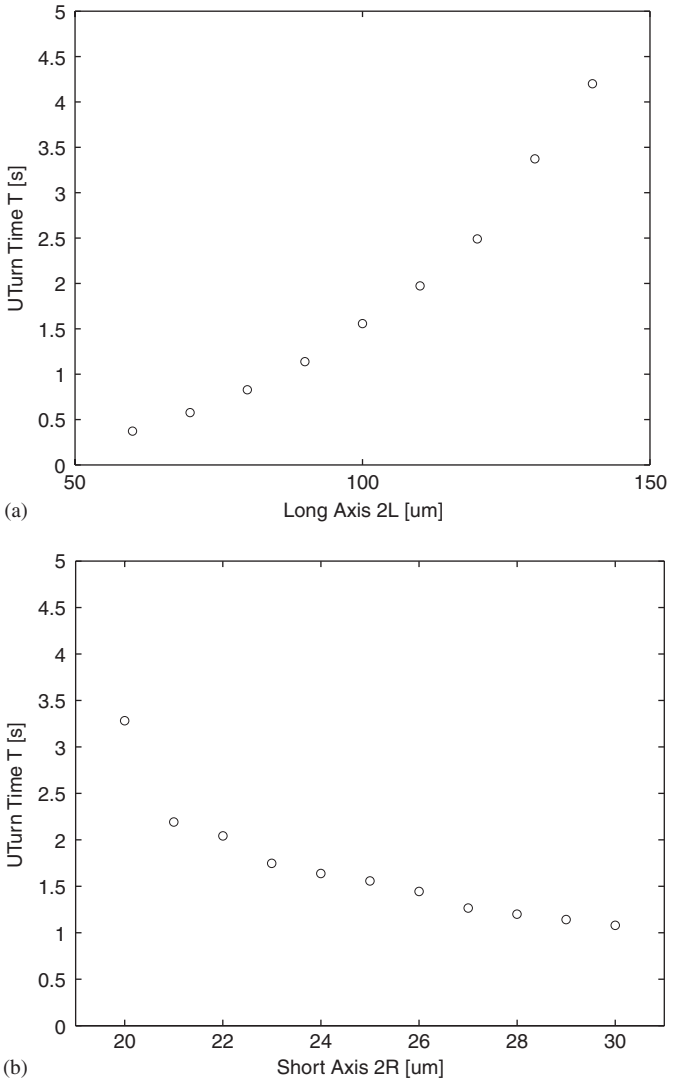

Fig. 10. Relationship between U-turn time and (a) L and (b) R. These graphs indicate that it takes more time for elongated cells to make a U-turn.

hydrodynamic viewpoint if more rigorous discussion is needed, which is not dealt with in this paper.

3.8. Comparison with experimental data

We have accumulated data for paramecia motion using a high-speed vision system called I-CPV (Toyoda et al., 2001), which was jointly developed by Hamamatsu Photonics K.K. and one of the authors (M. Ishikawa) of the present paper, and a galvanotaxis continuous observation system developed in our laboratory (Ogawa et al., 2004). We verified the validity of the model using these data.

3.8.1. Experimental setup

Experimental data were obtained by high-speed measurement of the responses of a single cell to an electric field, using the galvanotaxis continuous measurement system (Ogawa et al., 2004). The setup of the system is illustrated in Fig. 11.

Wild-type *P. caudatum* cells were cultured at 20–25 °C in a soy flour solution. Cells grown to the logarithmic or stationary phase (4–10 days after incubation) were collected together with the solution, filtered through a nylon mesh to remove debris, and infused into a chamber.

The chamber was planar with a depth of 0.17 mm in order to constrain the motion of the cells within a two-dimensional plane. The chamber was located between two parallel carbon electrodes 0.5 mm in diameter with a 22-mm gap between them, placed on a glass slide, in order to control the electrical stimulus in the direction perpendicular to the electrodes. In order to maintain the chamber depth and to suppress evaporation of the solution, a cover glass was placed on the chamber. A DC electric field with a step-like temporal profile rising to 4.1 V/cm was applied to the cells.

Cell position and angle were continuously measured at a 1-kHz frame rate using a high-speed lock-on tracking method (Oku et al., 2005; Ogawa et al., 2005). Lock-on tracking, which means keeping the target in the center of the image field, allows natural in vivo measurement of free-swimming motile cells without fixing them or slowing them down. Tracking was implemented by moving the chamber using an XY stage on which it was mounted, based on target information captured by the I-CPV high-speed vision system. The I-CPV system includes an image intensifier and a Column Parallel Vision (CPV) system, which is a high-speed vision system developed for robotic applications (Nakabo et al., 2000). It has a frame rate of 1 kHz and can execute various operations, such as global image feature extraction, edge extraction, embossing and blurring, within 1 ms. The I-CPV system was mounted on an upright optical microscope (Olympus, BX50WI) and captured dark-field images. From the captured images, the I-CPV obtained image features and sent them to a PC. These features were used for the visual feedback control of the XY stage and the applied electrical stimulus. Fig. 11C shows an example of the tracked image of a *Paramecium* cell making a U-turn.

3.8.2. Comparison of data

We compared simulated and experimental positions in the U-turn motion. We extracted positions along the electric field (X direction), because X-disposition is almost independent of fluctuations caused by spiral motions, which we disregarded.

Fig. 12 shows experimental data (thin lines) for three seconds from application of a stimulus (reversal of the electric field) in six trials. In the simulation (thick line), the initial angle was set to 33.6457°, which is the average of angles obtained from previously measured data. The field strength was set to 4.1 V/cm same as the wet experiment. The figure indicates that the simulated data was approximately in agreement with the experimental results.

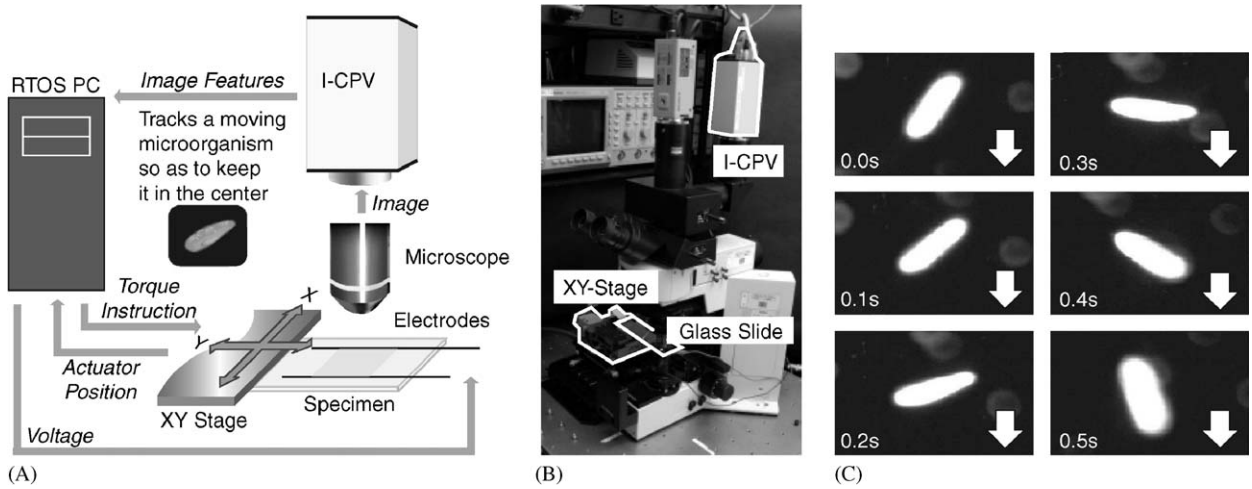

Fig. 11. Experimental setup of our tracking system. (A): Schematic overview of the galvanotaxis continuous observation system (Ogawa et al., 2004). Cells are infused into a planar chamber on a glass slide. Two electrodes apply an electric field to the chamber. The cell motion is tracked by the high-speed vision system I-CPV so as to keep the cell in the center of the microscope field; I-CPV captures the images with 1-kHz frame rate and calculates image features, which are used to control the XY stage. (B): Photograph of the system. (C): An example of U-turn motion observed by our system. Note that I-CPV does not provide the captured images to the outside, and these images were simultaneously captured by a branched CCD camera (this is why their aspect ratio is not 1:1). White arrows indicate the direction of the electric field.

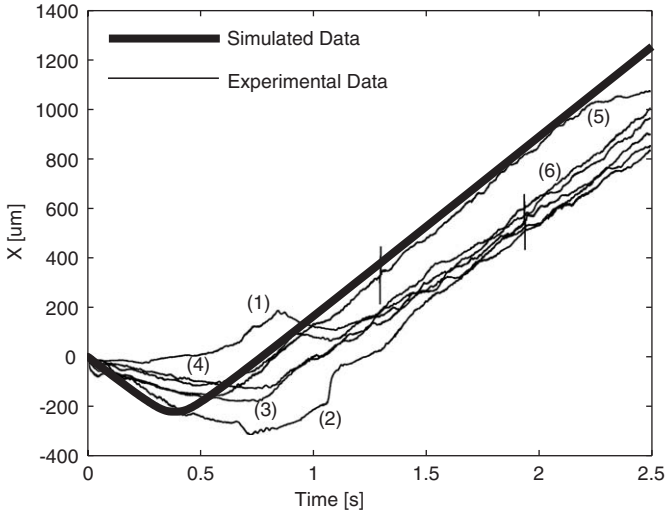

Fig. 12. Comparison between simulated data (thick line) and experimental data (thin lines) in the U-turn motion. Only the X-coordinates (positions along the electric field) are extracted. Experimental data for three seconds from the application of a stimulus in six trials are overlaid. In the experimental results, the initial angles were (1) 58.9055°, (2) 20.8729°, (3) 22.6034°, (4) 36.1584°, (5) 29.3349°, and (6) 33.9990°, respectively. In the simulation, the initial angle was 33.6457, which is the average of six angles obtained from previously measured data. The figure indicates that the simulated data was approximately in agreement with the experimental results.

This comparison is not a strict one because the experimental data represents the projection of real three-dimensional trajectories onto a two-dimensional plane. Although the planar structure of the chamber helps to restrict the vertical motion, the cell can still move slightly in this direction. A more rigorous comparison will require three-dimensional tracking. We are developing three-dimensional tracking methods for our work (Oku et al., 2004; Theodorus et al., 2005), and experiments are currently underway in our laboratory. Or the disparities might be due to stabilization time for the electrochemical phenomenon, which is supposed to be several hundred milliseconds, or the asymmetrical deviation of the cell shape (Mogami et al., 2001), though they are just a matter for speculation. We are planning to investigate it more precisely by wet experiments.

4. Conclusion

In this paper, we proposed a physical model of *Paramecium* galvanotaxis using a bottom–up approach to link the microscopic ciliary motion and the macroscopic behavior of a cell, and we investigated the validity of the model by numerical experiments.

One possible development of our model would be to incorporate physiological findings, regarded as black boxes in this paper. A complete framework from input to output, from the micro to macro scales, will provide a more accurate prediction of cell behavior. However, such work has a long way to go because some ion channels, including VDCCs, in *Paramecium* cells do not comply with simple conventional models such as the Hodgkin–Huxley equation[3] and details of their behavior remain unknown. As for ciliary movement, Naitoh and Kaneko (1973) reported that Ca^{2+} level rise affects axoneme movements, thus leading to ciliary reversal. cAMP and centrin are also essential to regulate ciliary movements (Satir et al., 1993; Gonda et al., 2004). We are planning to consider them from the viewpoint of system biology. Another interesting point to consider is stochastic

[3]Personal communications by Naitoh, Y. (2004), Kuroda, S. (2004), and Oosawa, F. (2005).

processes in the cells (Oosawa, 2001). The behavior of cells is not always deterministic and there is a wide diversity of behavior in paramecia. In addition, more comprehensive evaluation of the model based on three-dimensional data of cell trajectories will play an important role in future studies. Such work is currently underway in our laboratory.

Appendix A. Nomenclature

Variables	Definition
L	semimajor cell axis
R	semiminor cell axis
l	boundary plane offset
μ	water viscosity
ρ	cell density
β	beat frequency increase
X	X-position in global coordinate system
Y	Y-position in global coordinate system
$\boldsymbol{X}$	position in global coordinate system
ϕ	cell angle in global coordinate system
x	x-position in local coordinate system
y	y-position in local coordinate system
θ	electric field angle
$\boldsymbol{E}$	electric field vector
$\mathscr{E}$	cell ellipsoid
$\mathscr{L}$	boundary plane
n	cilia linear density
φ_0	beat frequency under $\boldsymbol{E}=\boldsymbol{0}$
φ	beat frequency under $\boldsymbol{E}$
f_0	force by single cilium under $\boldsymbol{E}=\boldsymbol{0}$
f	force by single cilium under $\boldsymbol{E}$
α	parameter between f and φ
x_+	x-coordinate of the intersection of $\mathscr{E}$ and $\mathscr{L}$ (with positive y-coordinate)
x_-	x-coordinate of the intersection of $\mathscr{E}$ and $\mathscr{L}$ (with negative y-coordinate)
w	the "height" of the trapezoid
$\mathrm{P}_{\{1,2\}}$	sites of action
$\boldsymbol{r}_{\{1,2\}}$	position vectors for $\mathrm{P}_{\{1,2\}}$
x_a	x-coordinate of $\mathrm{P}_{\{1,2\}}$
y_a	y-coordinate of $\mathrm{P}_{\{1,2\}}$
$\boldsymbol{F}_{\{1,2\}}$	resultant forces on $\mathrm{P}_{\{1,2\}}$
$\boldsymbol{m}_{\{1,2\}}$	tangent vectors on $\mathrm{P}_{\{1,2\}}$
$\boldsymbol{e}_{\{1,2\}}$	unit force vectors
$\boldsymbol{\tau}_{\{1,2\}}$	torques on $\mathrm{P}_{\{1,2\}}$
$\boldsymbol{\tau}$	whole torque
$\tau_z(\phi)$	z-component of $\boldsymbol{\tau}$
s	$\sin\phi$
c	$\cos\phi$
F	whole propulsion force
$\boldsymbol{F}$	whole propulsion force vector
F_s	force given by Stokes' law
τ_s	viscous resistant torque given by Stokes' law
Re	Reynolds number
v	cell velocity
v	dynamic viscosity of water
D	viscous friction coefficient
M	cell mass
V	cell volume
$\boldsymbol{e}$	unit vector parallel to the cell axis
δ	coefficient for compensate error
I	moment of inertia for ellipse
D'	viscous friction coefficient
$\boldsymbol{q}$	generalized coordinates
A	system matrix for $\boldsymbol{q}$
$\boldsymbol{B}$	input vector for $\boldsymbol{q}$
$\tilde{\boldsymbol{q}}$	part of $\boldsymbol{q}$
$\tilde{A}$	system matrix for $\tilde{\boldsymbol{q}}$
I_u	2×2 unit matrix
λ	variables for characteristic equation
P	coefficient for the propulsion force
Q	coefficient for the torque
U	potential energy
$\bar{X}$	spiral axis
$\bar{Y}$	an axis perpendicular to $\bar{X}$
$V_{\bar{X}}$	amplitude coefficient for $\bar{X}$
$V_{\bar{Y}}$	amplitude coefficient for $\bar{Y}$
ω	angular velocity of the spiral motion
$\bar{\phi}$	cell inclination with respect to $\bar{X}$
N	brown noise term

Appendix B. How to obtain x_a and w from x_+ and x_-

In this section, we describe briefly how to obtain x_a and w from x_+ and x_- by using Viète's Formulae.

Viète's Formulae, also used in Section 3.3, provide relationship between roots and coefficients in polynomial equations Viète, 1646; Waerden, 1977; Farkas and Farkas, 1975. The sum and product of the two roots of a quadratic equation are derived from coefficients.

Assume an n-degree polynomial equation:

$$a_n x^n + a_{n-1}x^{n-1} + \cdots + a_1 x + a_0 = (x-r_1)(x-r_2)\cdots(x-r_n) = 0.$$

Let S_i be a symmetric polynomial of the distinct polynomial roots, $r_1,\ldots,r_n$. For example, the first few values of S_i are:

$$S_1 = r_1 + r_2 + r_3 + r_4 + \cdots,$$

$$S_2 = r_1r_2 + r_1r_3 + r_1r_4 + r_2r_3 + \cdots,$$

$$S_3 = r_1r_2r_3 + r_1r_2r_4 + r_2r_3r_4 + \cdots.$$

Then the Viète's formulae state that:

$$S_i = (-1)^i \frac{a_{n-i}}{a_n}.$$

Particularly in a quadratic equation, this is expressed as:

$$S_1 = r_1 + r_2 = -\frac{a_1}{a_2},$$

$$S_2 = r_1 r_2 = \frac{a_0}{a_2}.$$

These were used in deriving x_a and w in the dynamics model of *Paramecium* in Section 2.3. From their definitions, x_a and w are written as:

$$x_a = \frac{x_- + x_+}{2},$$

$$w = x_- - x_+,$$

where x_+ and x_- are roots of the quadratic equation (3). By applying Viète's formulae to Eq. (3), we obtain:

$$x_+ + x_- = \frac{2lL^2 \cos\theta}{R^2 \sin^2\theta + L^2 \cos^2\theta},$$

$$x_+ x_- = \frac{l^2 L^2 - R^2 L^2 \sin^2\theta}{R^2 \sin^2\theta + L^2 \cos^2\theta},$$

$$x_- - x_+ = \pm\sqrt{(x_- + x_+)^2 - 4x_- x_+}.$$

Thus x_a and w are derived as:

$$x_a = \frac{lL^2 \cos\theta}{R^2 \sin^2\theta + L^2 \cos^2\theta},$$

$$w = \frac{2RL \sin\theta \sqrt{R^2 \sin^2\theta + L^2 \cos^2\theta - l^2}}{R^2 \sin^2\theta + L^2 \cos^2\theta},$$

where the sign of w is properly set to match consistency of the physical dynamics.

Appendix C. Asymptotic stability in dynamical systems

We briefly describe the asymptotic stability in dynamical systems theory.

In the differential equation

$$\frac{d\boldsymbol{x}(t)}{dt} = A\boldsymbol{x}(t), \tag{C.1}$$

if the solution $\boldsymbol{x}(t)$ converges to zero with $t \to 0$ for an arbitrary initial condition, the system is called asymptotically stable.

The general solution of Eq. (C.1) is:

$$\boldsymbol{x}(t) = e^{At}\boldsymbol{x}(0).$$

For simplicity, suppose that all eigenvalues of A, $\lambda_1, \lambda_2, \ldots, \lambda_n$, are discrete. Also, let $v_1, v_2, \ldots, v_n$ be eigenvectors of A. Then, $\exp(At)$ can be diagonalized as:

$$\begin{aligned} e^{At} &= \sum_{k=0}^{\infty} \frac{1}{k!}(At)^k \\ &= \sum_{k=0}^{\infty} \frac{1}{k!}(T\Lambda T^{-1}t)^k \\ &= T\left(\sum_{k=0}^{\infty} \frac{1}{k!}(\Lambda t)^k\right) T^{-1} \\ &= T\left(\mathrm{diag}(e^{\lambda_1 t}, \ldots, e^{\lambda_n t})\right) T^{-1} \end{aligned}$$

where $T = [v_1 \cdots v_n]$, and $\Lambda = \mathrm{diag}(\lambda_1, \ldots, \lambda_n)$ is a diagonal matrix of A. This shows that negative eigenvalues are necessary and sufficient condition for asymptotic convergence of $\boldsymbol{x}$ to zero as $t \to \infty$; if eigenvalues are non-negative, $\boldsymbol{x}$ will diverge exponentially. This is also true when eigenvalues are not discrete.

References

Anderson, J.D., 1951. Galvanotaxis of slime mold. J. Gen. Physiol. 35 (1), 1–16.

Bergethon, P.R., 1998. The Physical Basis of Biochemistry: The Foundations of Molecular Biophysics. Springer, New York.

Chiang, M., Robinson, K.R., Vanable Jr., J.W., 1992. Electrical fields in the vicinity of epithelial wounds in the isolated bovine eye. Exp. Eye Res. 54, 999–1003.

Cooper, M.S., Schliwa, M., 1985. Electric and ionic controls of tissue cell locomotion in DC electric fields. J. Neurosci. Res. 13, 223–244.

Djamgoz, M.B.A., Mycielska, M., Madeja, Z., Fraser, S.P., Korohoda, W., 2001. Directional movement of rat prostate cancer cells in direct-current electric field: involvement of voltage-gated Na^+ channel activity. J. Cell Sci. 114 (14), 2697–2705.

Eckert, R., Naitoh, Y., 1970. Passive electrical properties of *Paramecium* and problems of ciliary coordination. J. Gen. Physiol. 55 (4), 467–483.

Eckert, R., Naitoh, Y., 1972. Bioelectric control of locomotion in the ciliates. J. Protozool. 19 (2), 237–243.

Erickson, C.A., Nuccitelli, R., 1984. Embryonic fibroblast motility and orientation can be influenced by physiological electric fields. J. Cell Biol. 98 (1), 296–307.

Farkas, I., Farkas, M., 1975. Introduction to Linear Algebra. Adam Hilger, Bristol.

Fearing, R.S., 1991. Control of a micro-organism as a prototype micro-robot. In: Proceedings of Second International Symposium on Micromachines and Human Sciences.

Fukui, K., Asai, H., 1980. The most probable mechanism of the negative geotaxis of *Paramecium caudatum*. Proc. Japan Acad. Ser. B: Phys. Biol. Sci. 56 (B), 172–177.

Fukushima, K., Senda, N., Inui, H., Miura, H., Tamai, Y., Murakami, Y., 1953. Studies on galvanotaxis of leukocytes. I. Galvanotaxis of human neutrophilic leukocytes and methods of its measurement. Med. J. Osaka Univ. 4, 195–208.

Gonda, K., Yoshida, A., Oami, K., Takahashi, M., 2004. Centrin is essential for the activity of the ciliary reversal-coupled voltage-gated Ca^{2+} channels. Biochem. Biophys. Res. Comm. 323 (3), 891–897.

Görtz, H.-D., (Ed.), 1988. Paramecium. Springer, Berlin.

Gruler, H., Nuccitelli, R., 2000. The galvanotaxis response mechanism of keratinocytes can be modeled as a proportional controller. Cell Biochem. Biophys. 33, 33–51.

Hemmersbach, R., Krause, M., Bräucker, R., Ivanova, K., 2005. Graviperception in ciliates: steps in the transduction chain. Adv. Space Res. 35, 296–299.

Hirano, A., Tsuji, T., Takiguchi, N., Ohtake, H., 2005. Modeling of the membrane potential change of *Paramecium* for mechanical stimuli. Trans. SICE 41 (4), 351–357 (in Japanese).

Houten, J.V., Houten, J.V., 1982. Computer simulation of *Paramecium* chemokinesis behavior. J. Theor. Biol. 98, 453–468.

Ionides, E.L., Fang, K.S., Isseroff, R.R., Oster, G.F., 2003. Stochastic models for cell motion and taxis. J. Math. Biol. 48, 23–37.

Itoh, A., 2000. Motion control of protozoa for bio MEMS. IEEE/ASME Trans. Mech. 5 (2), 181–188.

Jahn, T.L., 1961. The mechanism of ciliary movement. I. Ciliary reversal and activation by electric current; the Ludloff phenomenon in terms of core and volume conductors. J. Protozool. 8 (4), 369–380.

Jennings, H.S., 1923. Behavior of the Lower Organisms. Columbia University Press, New York.

Kamada, T., 1929. Control of galvanotropism in *Paramecium*. J. Fac. Sci. Imp. Univ. Tokyo, Sect. IV, Zoology 2, 123–139.

Kamada, T., 1931a. Polar effect of electric current on the ciliary movements of *Paramecium*. J. Fac. Sci. Imp. Univ. Tokyo, Sect. IV, Zoology 2, 285–298.

Kamada, T., 1931b. Reversal of electric polar effect in *Paramecium* according to the change of current strength. J. Fac. Sci. Imp. Univ. Tokyo, Sect. IV, Zoology 2, 299–307.

Kinosita, H., 1939. Electrical stimulation of *Paramecium* with linearly increasing current. J. Cell. Comp. Physiol. 13 (3), 253–261.

Korohoda, W., Mycielska, M., Janda, E., Madeja, Z., 2000. Immediate and long-term galvanotactic responses of *Amoeba proteus* to dc electric fields. Cell Motil. Cytoskel. 45, 10–26.

Laurent, M., Fleury, A., 1995. A model with excitability and relay properties for the generation and the propagation of a Ca^{2+} morphogenetic wave in *Paramecium*. J. Theor. Biol. 174, 227–236.

Levin, M., 2003. Bioelectromagnetics in morphogenesis. Bioelectromagnetics 24, 295–315.

Ludloff, K., 1895. Untersuchungen über den Galvanotropismus. Arch. Ges. Physiol. 59, 525–554.

Machemer, H., 1974. Frequency and directional responses of cilia to membrane potential changes in *Paramecium*. J. Comp. Physiol. 92, 293–316.

Machemer, H., 1976. Interactions of membrane potential and cations in regulation of ciliary activity in *Paramecium*. J. Exp. Biol. 45 (2), 427–448.

Machemer, H., de Peyer, J., 1977. Swimming sensory cells: electrical membrane parameters, receptor properties and motor control in ciliated Protozoa. Ver. Deut. Zool. gesell. 86–110.

McCaig, C.D., Rajnicek, A.M., Song, B., Zhao, M., 2005. Controlling cell behavior electrically: current views and future potential. Physiol. Rev. 85, 943–978.

Mogami, Y., Ishii, J., Baba, S.A., 2001. Theoretical and experimental dissection of gravity-dependent mechanical orientation in gravitactic microorganisms. Biol. B. 201, 26–33.

Mycielska, M.E., Djamgoz, M.B.A., 2004. Cellular mechanisms of direct-current electric field effects: galvanotaxis and metastatic disease. J. Cell Sci. 117, 1631–1639.

Naitoh, Y., Kaneko, H., 1972. Reactivated Triton-extracted models of *Paramecium*: modification of ciliary movement by calcium ions. Science 176, 523–524.

Naitoh, Y., Kaneko, H., 1973. Control of ciliary activities by adenosine-triphosphate and divalent cations in Triton-extracted models of *Paramecium caudatum*. J. Exp. Biol. 58 (3), 657–676.

Naitoh, Y., Sugino, K., 1984. Ciliary movement and its control in *Paramecium*. J. Protozool. 31 (1), 31–40.

Naitoh, Y., Eckert, R., Friedman, K., 1972. A regenerative calcium response in *Paramecium*. J. Exp. Biol. 56, 667–681.

Nakabo, Y., Ishikawa, M., Toyoda, H., Mizuno, S., 2000. 1 ms column parallel vision system and it's application of high speed target tracking. In: Proceedings of 2000 IEEE International Conference on Robotics and Automation (ICRA2000), pp. 650–655.

Oertel, D., Schein, S.J., Kung, C., 1978. A potassium conductance activated by hyperpolarization in *Paramecium*. J. Mem. Biol. 43 (2–3), 169–185.

Ogawa, N., Oku, H., Hashimoto, K., Ishikawa, M., 2004. Single-cell level continuous observation of microorganism galvanotaxis using high-speed vision. In: Proceedings of 2004 IEEE International Symposium on Biomedical Imaging (ISBI 2004), pp. 1331–1334.

Ogawa, N., Oku, H., Hashimoto, K., Ishikawa, M., 2005. Microrobotic visual control of motile cells using high-speed tracking system. IEEE Trans. Robotics 21 (4), 704–712.

Ohtake, H., Yako, T., Tsuji, T., Kato, J., Kuroda, A., Kaneko, M., 1997. An approach to molecular artificial life: bacterial intelligent behavior and its computer model. In: Langton, C.G., Shimohara, K. (Eds.), Artificial Life V: Proceedings of Fifth International Workshop on the Synthesis and Simulation of Living Systems. MIT Press, Cambridge, MA, pp. 395–401.

Oku, H., Hashimoto, K., Ishikawa, M., 2004. Variable-focus lens with 1-kHz bandwidth. Opt. Express 12 (10), 2138–2149.

Oku, H., Ogawa, N., Hashimoto, K., Ishikawa, M., 2005. Two-dimensional tracking of a motile micro-organism allowing high-resolution observation with various imaging techniques. Rev. Sci. Instrum. 76 (3).

Oosawa, F., 1975. The effect of field fluctuation on a macromolecular system. J. Theor. Biol. 52, 175–186.

Oosawa, F., 2001. Spontaneous signal generation in living cells. B. Math. Biol. 63, 643–654.

Oosawa, F., Nakaoka, Y., 1977. Behavior of micro-organisms as particles with internal state variables. J. Theor. Biol. 66, 747–761.

Orida, N., Feldman, J.D., 1982. Directional protrusive pseudopodial activity and motility in macrophages induced by extracellular electric fields. Cell Motil. Cytoskel. 2 (3), 243–255.

Roberts, A.M., 1970. Motion of *Paramecium* in static electric and magnetic fields. J. Theor. Biol. 27, 97–106.

Robinson, K.A., 1985. The responses of cells to electrical fields: a review. J. Cell Biol. 101 (6), 2023–2027.

Sakane, A., Hashigami, K., Tsuji, T., Ohtake, H., Kaneko, M., 2001. Model of taxis of Paramecia based on the Hodgkin–Huxley equations. In: Proceedings of 2001 JSME Conference on Robotics and Mechatronics (Robomec'01), pp. 2P2–B9, in Japanese.

Satir, P., Barkalow, K., Hamasaki, T., 1993. The control of ciliary beat frequency. Trends Cell Biol. 3 (11), 409–412.

Schienbein, M., Gruler, H., 1993. Langevin equation, Fokker–Planck equation and cell migration. B. Math. Biol. 55 (3), 585–608.

Shi, W., Stocker, B.A.D., Adler, J., 1996. Effect of the surface composition of motile *Escherichia coli* and motile *Salmonella* species on the direction of galvanotaxis. J. Microbiol. 178 (4), 1113–1119.

Sugino, K., Naitoh, Y., 1982. Simulated cross-bridge patterns corresponding to ciliary beating in *Paramecium*. Nature 295, 609–611.

Theodorus, Oku, H., Hashimoto, K., Ishikawa, M., 2005. Optical axis tracking of microorganism using high-speed vision. In: Proceedings of Focus on Microscopy 2005.

Toyoda, H., Mukohzaka, N., Nakamura, K., Takumi, M., Mizuno, S., Ishikawa, M., 2001. 1 ms column-parallel vision system coupled with an image intensifier; I-CPV. In: Proceedings of Symposium on High Speed Photography and Photonics 2001, vol. 5(1), pp. 89–92 (in Japanese).

Verworn, M., 1889. Die polare Erregung der Protisten durch den galvanischen Strom. Arch. Ges. Physiol. 45, 1–36.

Verworn, M., 1896. Untersuchungen über die polare Erregung der lebendigen Substanz durch den constanten Strom. III. Mittheilung. Arch. Ges. Physiol. 62, 415–450.

Viète, F., 1646. Francisci Vietae Opera Mathematica. Leiden.

Waerden, B.L.v., 1977. Algebra, vol. 1. Frederick Ungar Publishing Co., New York.

Yamane, J., Ogawa, N., Oku, H., Hashimoto, K., Ishikawa, M., 2004. A current controlled electrostimulation device for the motion control of Paramecia. In: Proceedings of 2004 JSME Conference on Robotics and Mechatronics (Robomec'04), pp. 1A1-H-28 (in Japanese).

Zhang, X., Jin, L., Takenaka, I., 2000. Galvanotactic response of mouse epididymal sperm: in vitro effects of zinc and diethyldithiocarbamate. Archiv. Androl. 45, 105–110.

Zhao, M., Jin, T., McCaig, C.D., Forrester, J.V., Devreotes, P.N., 2002. Genetic analysis of the role of G protein-coupled receptor signaling in electrotaxis. J. Cell Biol. 157 (6), 921–927.